Chemical Engineering Science 260 (2022) 117920

Contents lists available at ScienceDirect

Chemical Engineering Science

journal homepage: www.elsevier.com/locate/ces

Microreactor technology in experimental and modelling study of alcohol oxidation on nanogold

Luca Mastroianni [a,b], Zuzana Vajglová [a], Kari Eränen [a], Markus Peurla [c], Martino Di Serio [b], Dmitry Yu. Murzin [a], Vincenzo Russo [a,b], Tapio Salmi [a,*]

[a] Åbo Akademi University, Laboratory of Industrial Chemistry and Reaction Engineering (TKR), FI-20500 Turku/Åbo, Finland
[b] Università di Napoli "Federico II", Chemical Sciences Department, IT-80126 Napoli, Italy
[c] University of Turku, Laboratory of Electron Microscopy, Department of Industrial Physics and Astronomy, FI-20500 Turku/Åbo, Finland

HIGHLIGHTS

- Microreactor channels were coated with Au/γ-Al_2O_3 catalyst.
- The presence of active gold nanoparticles was confirmed.
- Selective oxidation of methanol, ethanol, propanol and butanol was successfully conducted and modelled mathematically.
- The role of intrawashcoat diffusion in the catalyst layer was revealed.

ARTICLE INFO

Article history:
Received 20 April 2022
Received in revised form 7 June 2022
Accepted 14 July 2022
Available online 19 July 2022

Keywords:
Microreactor
Gold catalyst
Nanoparticles
Alcohol oxidation
Reaction mechanism
Kinetic modelling

ABSTRACT

Selective oxidation of methanol, ethanol, 1-propanol and 1-butanol to corresponding aldehydes was performed in a microreactor in the presence of a Au/γ-Al_2O_3 coated catalyst. Nanoparticle size distribution, acidity, specific surface area and the average pore size as well as uniformity and thickness of the coating layer were evaluated with relevant characterization techniques. The experiments were designed to reveal the effect of temperature, residence time and oxygen-to-alcohol ratio on both alcohol conversion and product distribution. Stability and repeatability of the coating procedure was successfully demonstrated. To describe the reaction kinetics, plausible kinetic equations were implemented in a pseudo-homogeneous plug flow model, which turned out to be an adequate approximation to describe the flow pattern in the microreactor. Non-linear regression analysis enabled the determination of the rate and adsorption parameters included in the kinetic model. An advanced kinetic and mass transfer model was developed to reveal the impact of the diffusion inside the catalytic washcoat layer, confirming that molecular diffusion is not a limiting factor for alcohol oxidation in the microreactor.

1. Introduction

Partial oxidation of primary alcohols to produce aldehydes is one of the key reactions in organic chemistry (Sheldon et al., 2002). Molecular oxygen represents a clean alternative to the traditionally employed chromium-based stoichiometric reagents, which are harmful for both human beings and environment. According to guidelines of green chemistry, heterogeneous catalysts should be preferred to stoichiometric reagents (Anastas and Warner, 1988), allowing more efficient catalyst separation and atom efficiency.

Gold nanoparticles (AuNPs) dispersed onto support materials are acknowledged to be highly active and selective catalysts in selective oxidation processes (Behravesh et al., 2018, Sharma et al., 2016, Abad et al., 2008). As early as in 1913, Fokin (1913) successfully employed gold in the catalytic oxidation of methanol to formaldehyde, demonstrating its activity for the first time. However, the catalytic properties of gold were forgotten by the scientific community in the years later. The scenario dramatically changed as Haruta et al. (1985) and Hutchings (1987) discovered the activity of gold in the catalytic oxidation of CO and catalytic hydrochlorination of acetylene respectively, triggering the interest

* Corresponding author.
E-mail address: tapio.salmi@abo.fi (T. Salmi).

https://doi.org/10.1016/j.ces.2022.117920
0009-2509/

Notation

Latin letters

a_k	Activity of the catalyst for the alcohol k
$C_{0,i}$	Inlet concentration of the component i
C_i	Concentration of the component i in the gas-phase
$C_{s,i}$	Concentration of the component i in the gas-phase
$D_{A,B}$	Molecular diffusion of the component A in B
$D_{eff,i}$	Effective diffusivity of the component i
$E_{a,j}$	Activation energy of the reaction j
$K_{eq,j}$	Equilibrium constant of the reaction j
K_k^G	Adsorption coefficient of the alcohol k on the surface of gold
K_k^L	Adsorption coefficient of the alcohol k on Lewis sites of alumina
$K_{O_2}^G$	Adsorption coefficient of oxygen on the surface of gold
k_j	Kinetic constant of the reaction j
$k_{ref,j}$	Kinetic constant of the reaction j at the reference (depend on the reaction order)
L_r	Channel length
M_i	Molecular weight of the component i
p_k	Partial pressure of the alcohol k
Q_g	Volumetric flow rate
R	Gas constant
r_j	Reaction rate
R_w	Washcoat thickness
s	Shape factor
S_i	Selectivity to the product i
T	Temperature
T_{ref}	Reference Temperature
TOF	Turnover frequency
TOS	Time on stream
u_g	Gas velocity
X_k	Conversion of the alcohol k
x	Dimensionless axial coordinate

Greek letters

$\Delta_f G_i^0$	Gibbs free energy of formation of the component i at standard conditions
$\Delta_r G_j^0$	Gibbs free energy of reaction j at standard conditions
$\Delta_r G_j$	Gibbs free energy of reaction j at 1 bar a chosen temperature
$\Delta_f H_i^0$	Enthalpy of formation of the component i at standard conditions
$\Delta_r H_j^0$	Enthalpy of the reaction j at standard conditions
ρ_b	Bulk density
v_i	Atomic diffusion volume increment of the component i
ν_{ij}	Element of the stoichiometric matrix
τ	Residence time
χ	Dimensionless washcoat coordinate

of academic researchers in catalytic oxidation processes promoted by gold (Tabakova, 2019). The outstanding properties of gold has been observed only in nanoparticles and evidently they disappear in the micrometric scale (Corma and Garcia, 2008). Therefore, the recent impetus of nanoscience and the modern synthesis techniques of supported nanoparticles have been the driving force for the development of this new field of catalysis.

Various selective oxidation processes can be efficiently catalysed by gold nanoparticles. Partial oxidation of methanol produces formaldehyde, which is an essential chemical building block in several industrial applications (Salthammer et al., 2010). Bioethanol is regarded as a sustainable alternative to ethylene in the synthesis of acetaldehyde, typically performed by the Wacker process (Xu J. et al., 2016). Partial oxidation of 1-propanol gives access to propanal, which is a key intermediate in the manufacturing of rubber, plasticizers and paints (Gong et al., 2020). Alkyd resins, polyurethanes and lubricants can be obtained by using butanal (Mascal, 2012), which is the oxidation product of butanol. In all the oxidation processes presented above, industrial scale application of gold nanoparticles as active phases is of great interest.

Besides the catalyst material, the reactor structure is of great importance in the design of partial oxidation processes. For continuous gas-phase processes, packed bed reactors are often used. Moreover, in order to keep the pressure drop in the reactor under control, large catalyst particles ($\gg$ 1 mm) have to be used, which limits the efficiency because of heavy diffusion limitation. Therefore, structured reactors with thin catalyst layers have been developed, such as monoliths, solid foams and microreactors.

Microreactors have emerged as a promising technology in process intensification. The high area-to-volume ratio in microreactors enables very efficient heat transfer, allowing quasi-isothermal operations in the presence of highly exothermic and endothermic reactions. Diffusion of the molecules is rapid because of the micrometre dimension of the channels and thin catalyst layers, leading to the suppression of internal and external mass-transfer limitations. Therefore, microreactors are excellent tools to measure intrinsic kinetics for rapid gas-phase processes (Salmi et al., 2019, Schmidt et al., 2013). When using microreactors, the scale-up i.e., increasing the production capacity from the laboratory (g/min) to the industrial scale (ton/h), is in principle very straightforward. Several small units can be installed in parallel to increase the productivity to the desired production level. This procedure is usually referred as "numbering-up". The hydrodynamic and transfer characteristics of the laboratory scale devices are preserved with this procedure. However, hundreds of thousands of microreactors might be needed to satisfy the demand in case of bulk chemicals. Moreover, many advanced flow distributors and gas delivery systems (e.g., mass flow controllers) are required to ensure a uniform fluid flow in each reaction module. Thus, the microreactor scale-up remains a challenging task and cannot be regarded as a simple number up problem only. To reach a long-term industrial feasibility, numbering up might be combined with sizing up, i.e., increasing the length and/or the diameter of the channels (Dong et al., 2021). At the current state of art, microreactors are a powerful tool for laboratory scale kinetic studies. Also, they can meet the industrial needs for production capacities up to 1000 t/a (Salmi et al., 2019).

The goal of this work was to determine the reaction kinetics and product distribution in the oxidation of methanol, ethanol, 1-propanol and 1-butanol on gold nanoparticles deposited in a laboratory scale microreactor structure. The same reaction conditions were investigated for all the alcohols in a systematic approach aimed to correlate the catalyst activity with the chain length of the primary alcohols. Mathematical modelling based on plausible reaction mechanisms was carried out to reveal kinetic and adsorption parameters. An advanced kinetic and mass transfer model was developed to reveal the impact of the diffusion in the catalyst layer.

2. Experimental section

2.1. Microreactor coating

The Au/γ-Al_2O_3 catalyst employed for oxidation of L-arabinose to arabinoic acid was used. The direct ion exchange (DIE) method

was applied, in which an $HAuCl_4$ aqueous precursor solution was heated up at 70 °C and mixed with γ-Al_2O_3. Ammonia was used as the washing agent. Further details about the catalyst preparation can be found in Simakova et al. (2011).

The microreactor channels were successfully coated with the slurry-based method described in the literature (Behravesh et al., 2019, Schmidt et al., 2012, Vajglová et al., 2018, Suerz et al., 2021). First, the catalyst powder was finely grinded and sieved to obtain solid particles with the diameter less than 32 μm. A 5 wt% Au/γ-Al_2O_3 slurry was prepared by mixing 0.21 g of the catalyst in 4 mL of water. The pH of the slurry was adjusted with an ammonium hydroxide (32 %, Merck) solution at the value of 9.2. Then, the slurry was mixed with a magnetic stirrer for 4 h at 50 °C and afterwards at room temperature for four days at the rotation speed of 500 rpm. Prior to the coating, neat microplates were thermally pre-treated at 750 °C in the presence of air, creating an oxide layer on the surface which increased the surface roughness and, consequently, the catalyst adhesiveness. The slurry was withdrawn with a Finnpipette (0.5–5 μL) and deposited into the channels of the microreactor. The coated platelets were dried at 5 °C for seven hours, after which the excess of catalyst was scratched of with a spoon. For a further drying of the plates, they were placed in an oven at 100 °C for seven hours. Finally, the microplates were calcined at 300° C.

2.2. Catalyst and coating characterization

To obtain information about the catalyst and coating properties, various characterization techniques were applied. They are summarized briefly here.

TEM (JEOL JEM-1400Plus) was employed to evaluate the Au nanoparticle distribution. The analyses were conducted on the raw powder catalyst and on the particles present in the slurry after four days of stirring in the basic solution. The excess of suspension was dried overnight at 100 °C prior to the analysis. The spent catalyst was also analyzed after scratching few particles from the spent microplates. SEM was applied to measure the crystal size distribution and investigate the catalyst surface morphology before and after the coating procedure.

Nitrogen physisorption (Micromeritics 3 Flex 3500) was used to determine the surface area of both the raw powder catalyst and the catalyst contained in the slurry after four days of aging in the basic solution. The Brønsted and Lewis acidities were quantitatively determined with an Infrared Spectroscopy (ATI Mattson – Infinity Series) by using pyridine as the probe molecule. Thin catalyst pellets of 14 mg were prepared prior to the analysis. To obtain information about the strength of the acid sites, measurements at 250 °C (weak + medium + strong sites), 350 °C (medium + strong sites) and 450 °C (strong sites) were conducted. The results were interpreted by using the extinction coefficient reported in the work of Emeis (1993). An optical microscope was used to determine the uniformity of the catalyst coating of the microchannels.

2.3. Equipment and procedures for kinetic experiments

2.3.1. Gas-phase microreactor equipment

The kinetic investigations were conducted in a gas-phase microreactor purchased from Institut für Mikrotechnik Mainz GmbH (IMM), comprising ten stainless-steel microplates with nine channels each. The coated microplates were installed in parallel into the microreactor housing (Figure S1a) and mixing of the reactants was ensured by ten microstructured mixing plates located in front of the catalytic zone (Figure S1b-S1d). Two cylindrical cartridges heated up the system at the desired temperature, which was controlled by a PID controller (CalControls 9500P) and measured with a thermocouple. The characteristic dimensions of the microreactor are summarized in Table 1.

Table 1
Microreactor properties.

Property	Value
Size (L × B × H) (mm)	45 × 45 × 32
Connectors (inlet/outlet)	1/4''
Number of mixing plates	10
Size of mixing plates (mm)	7.5 × 7.5
Number of catalyst plates	10
Size of catalyst plate (mm)	9.5 × 9.5
Channel geometry of the catalyst plates (width × depth; μm)	460 × 90
Numers of channels per plate	9

Neat alcohol was fed from the bottom with a syringe pump (Fusion 200) as a liquid and mixed with helium that carried the reactant to the pre-heater, where the alcohol was slowly vaporized keeping the temperature few degrees below the boiling point of the alcohol. More aggressive vaporization would have been undesirable generating non–homogeneous gas flows. Oxygen was fed from the top with an additional helium flow. A flow sheet of the experimental equipment is illustrated in Fig. 1.

2.3.2. Alcohol oxidation experiments

The effect of temperature, residence time, the oxygen-to-alcohol molar ratio and the alcohol inlet concentration was investigated in the microreactor using identical conditions for all the alcohols.

The reaction temperature was varied within the range 200 – 350 °C, while the volumetric flow rate was 25–100 mL min^{-1}, implying that the residence time in the microreactor channels was 0.02 – 0.07 s. The alcohol inlet concentration, in terms of the partial pressure, was varied from 0.12 atm to 0.23 atm. For a given primary alcohol, the stoichiometry of selective oxidation towards the correspondent aldehyde can be written as.

$$R\text{-}CH_2OH + 0.5\ O_2 \rightarrow R\text{-}CHO + H_2O$$

In this work, the oxygen-to-alcohol ratio was varied from the stoichiometric one to four times oxygen excess. The complete experimental matrix is reported in supplementary material (Table S1).

2.3.3. Coating stability and repeatability

To investigate the long- term stability of the catalytic coating, a reference experiment for each alcohol was repeated periodically during the experimental campaign. During the tests, the temperature was set at 300 °C, the flow rate at 50 mL/min, the alcohol inlet partial pressure was 0.21 atm and with the oxygen-to-alcohol ratio of 2. Moreover, the coating reproducibility was studied by repeating the coating procedure on fresh microplates. Butanol was chosen as the substrate to check the coating repeatability at the operating conditions used in the reference experiment. In butanol oxidation, the fresh coating was used to investigate the effect of the reactant concentrations. To compare the catalyst performance after different coating procedures, the nomenclature "coating 1" and "coating 2" was applied.

3. Experimental results and discussion

3.1. Catalyst and coating properties

The influence of gold deposition and slurry preparation on Brønsted and Lewis acidities of γ-Al_2O_3 is displayed in Table 2.

As expected, the surface of alumina mainly consist of Lewis acid sites. Gold deposition increased significantly the Lewis acidity as

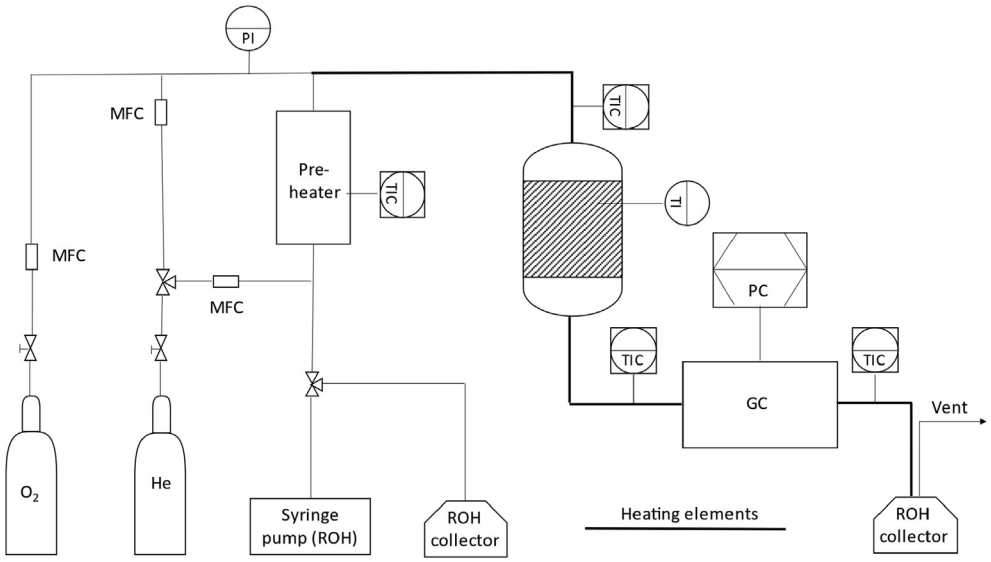

Fig. 1. Schematic process flow diagram for alcohol oxidation in microreactor.

Table 2
Acidity of the unsupported γ-Al_2O_3 and Au/γ-Al_2O_3 before and after ageing.

Catalyst	Brønsted acid sites [μmol/g]				Lewis acid sites [μmol/g]			
	weak	medium	strong	∑	weak	medium	strong	∑
γ-Al_2O_3	4	0	0	4	28	11	0	38
Au/γ-Al_2O_3	4	2	0	6	58	5	1	64
4 days aged	0	0	0	0	33	21	0	54

gold nanoparticles are electron acceptors, therefore acting as Lewis acid sites (Behravesh et al., 2017). In basic solutions, alumina hydration, dissolution and subsequent aluminium hydroxide precipitation were observed in previous studies; therefore, changes in the distribution of Lewis acid sites after slurry preparation can be ascribed to the morphological changes of alumina. Surface area has also been affected by the coating procedure to a small extent as it was 200 m^2/g and 225 m^2/g in the raw powder and in the aged catalyst, respectively.

Very small gold clusters of average size of 2 nm were observed in the powder catalyst (Fig. 2). The treatment with a base led to nanoparticle agglomeration, probably because of the increased mobility of the gold nanoparticles while the alumina structure was modified. Particles>12 nm were detected in the spent catalysts, meaning that butanol oxidation led to pronounced particle sintering.

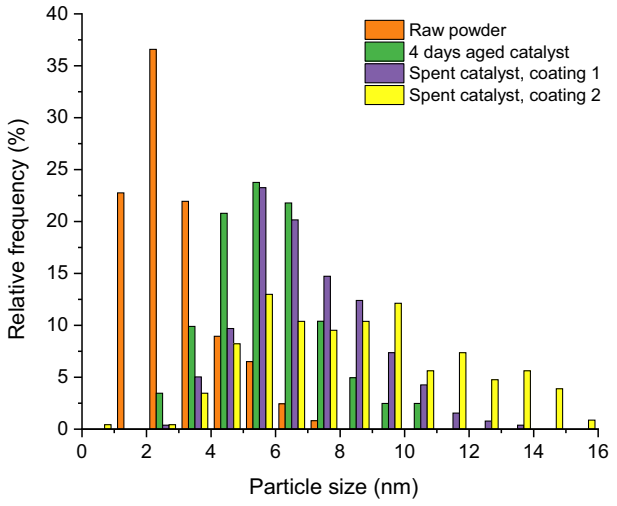

Fig. 2. Gold nanoparticle distribution.

Stirring in a basic solution causes a catalyst particle deagglomeration, changing rheological properties of the viscous slurry thus improving the coating performance (Behravesh et al., 2019). SEM micrographs confirmed that the catalyst average particle size decreased from 6 to 1 μm after stirring (Fig. 3).

Optical microscope images and SEM micrographs applied on the coated microplates confirmed successful coating (Fig. 4, S2-S3). The catalyst was uniformly distributed in the microreactor channels as neither scratches nor empty spaces were observed. The measured coating layer thickness was 8 ± 1 μm; therefore, the diffusional path inside the coating layer was very small, leading to suppression of the diffusion resistance enabling the investigation of the intrinsic kinetics of the reactions. Indeed, assuming an effective diffusion coefficient in the catalyst layer D_{eff} = 10^{-6} m^2/s, the average intrawashcoat diffusion time is 0.06 ms, which is about five hundred times lower than the estimated average residence time (40 ms). Even though this is evidence of how powerful the microreactor technology is in eliminating intraparticle diffusion limitations, it might not be enough to exclude it for extremely rapid reactions. In this case, the intrawashcoat concentration profiles should be examined with the aid of advanced mathematical models based on the concept of simultaneous reaction and diffusion in porous layers.

3.2. Catalyst performance in alcohol oxidation

3.2.1. Reaction networks

The reaction network observed for oxidation of different alcohols is displayed in Fig. 5 reflecting the formed products.

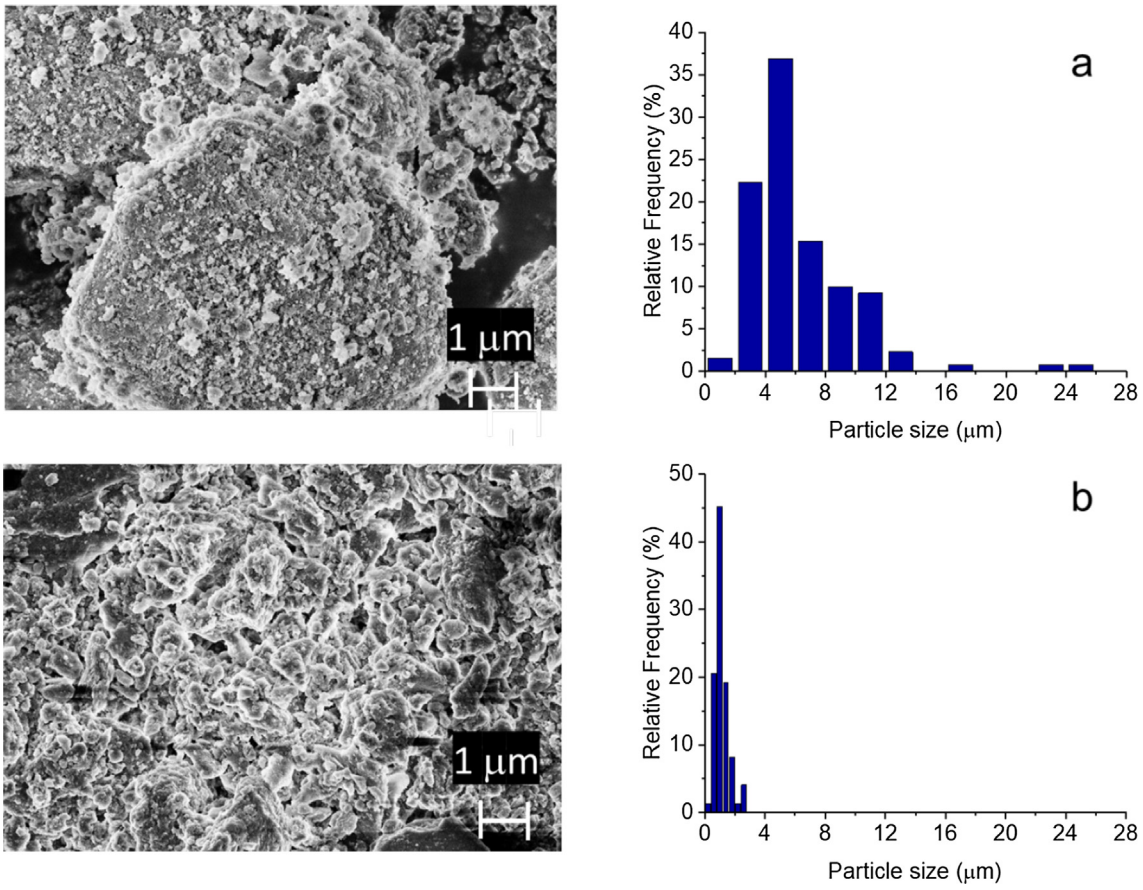

Fig. 3. Particle size distribution of (a) raw powder and (b) four days aged catalyst.

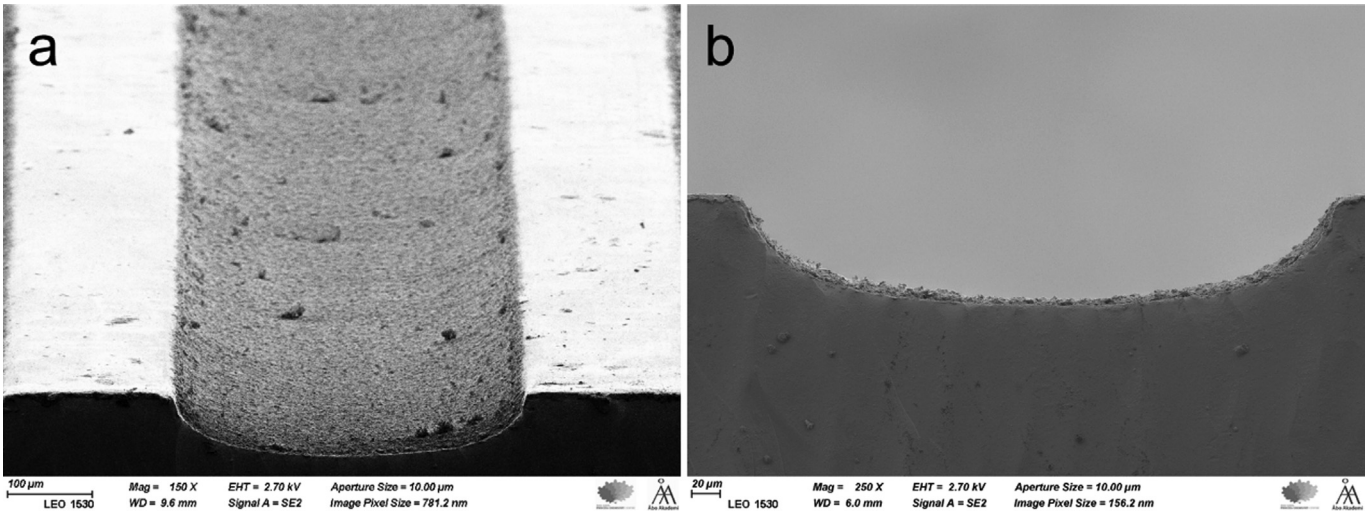

Fig. 4. (a) microreactor channel (b) coating frontal view.

Ethanol, propanol and butanol oxidation comprises three parallel reactions (Fig. 5b); together with aldehyde formation, etherification and alkene formation took place simultaneously. A higher reactivity of methanol led to a more complex product distribution as CO, CO_2 and methyl formate were detected in non-negligible amounts. Thermodynamic calculations suggested that etherification reaction is reversible within the temperature range investigated, while other reactions comprising the networks are irreversible. As a matter of fact, the estimated equilibrium constants of etherification were small, showing values lower than unity. On the contrary, the oxidation reactions present a very high value of the equilibrium constant ($K_{eq,j} > 10^6$). Detailed information about reaction thermodynamics is reported in the supplementary material (Tables S8-S9).

3.2.2. Coating stability and reproducibility

The catalyst coating used in the complete investigation of methanol, ethanol and, partially, in butanol oxidation (coating 1)

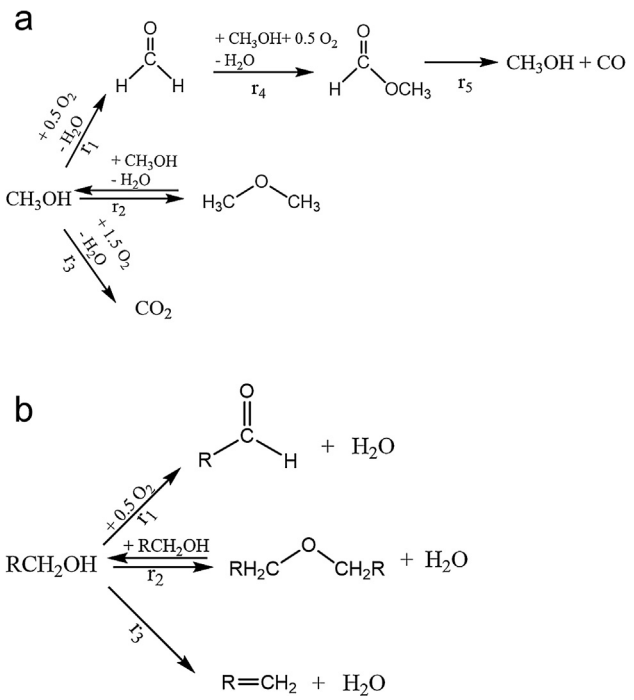

Fig. 5. Reaction network in (a) methanol oxidation (b) ethanol, propanol and butanol oxidation.

was very stable over one month of operation (Fig. 6). The TEM micrographs however indicated some sintering effects in the spent catalyst (Fig. 2). Reasonably, they can be ascribed to butanol oxidation, in which a decline of catalyst activity has been detected (Fig. 6d-7a).

The calculated catalyst amount in the microreactor in coating 1 was 4 mg, while it was 5 mg in the coating 2. Therefore, activity per unit of the catalyst mass was used to compare the catalyst performance within different slurry preparations, thus testing the coating repeatability. Fig. 7a confirmed the outstanding repeatability of the kinetic experiments in the application of microreactor technology. Since the catalyst amount was slightly higher in coating 2, the butanol conversion was also improved; however, this led to a slightly different product distribution (Fig. 7b). Moreover, the selectivity towards butanal decreased to a small extent, probably because of the nanoparticle sintering (Fig. 2).

3.2.3. Kinetic investigation results

Following the Arrhenius law, the dependence of the alcohol conversion on temperature exhibited a typical exponential behaviour (Fig. 8a). Because the volumetric flow rate is inversely proportional to the residence time, a decrease in alcohol conversion was observed as the volumetric flow was augmented. Up to 300 °C, the catalytic activity decreased in the order:

$$a_{\mathrm{MetOH}} > a_{\mathrm{EtOH}} > a_{\mathrm{PropOH}} \approx a_{\mathrm{ButOH}}$$

A decline of the alcohol reactivity with the chain length was also reported by Wang and Ueda (2008) in the aerobic oxidation of alcohols over Mo-V-O oxides. They suggested that the sterical hindrance of the alcohol chain length is an important factor to explain catalytic activity. Conversely, Corma et al. (1996) noted an increase of the reactivity with the chain length when oxidizing alcohols with hydrogen peroxide over TS-1. The catalytic behaviour of the alcohol oxidation was in line with the predicted intermediate on the active sites of TS-1. In the aereobic oxidation of alcohols promoted by gold, the formation of alkoxy species is supposed to occur on the catalytic surface (Behravesh et al., 2021, Boronat et al., 2011). The inductive effect of the alkyl chain length diminishes the electrophilicity of the hydroxyl group, lowering the reactivity of the reaction intermediate. Mathematical modelling confirmed a decrease of the adsorption constant of the alcohol on

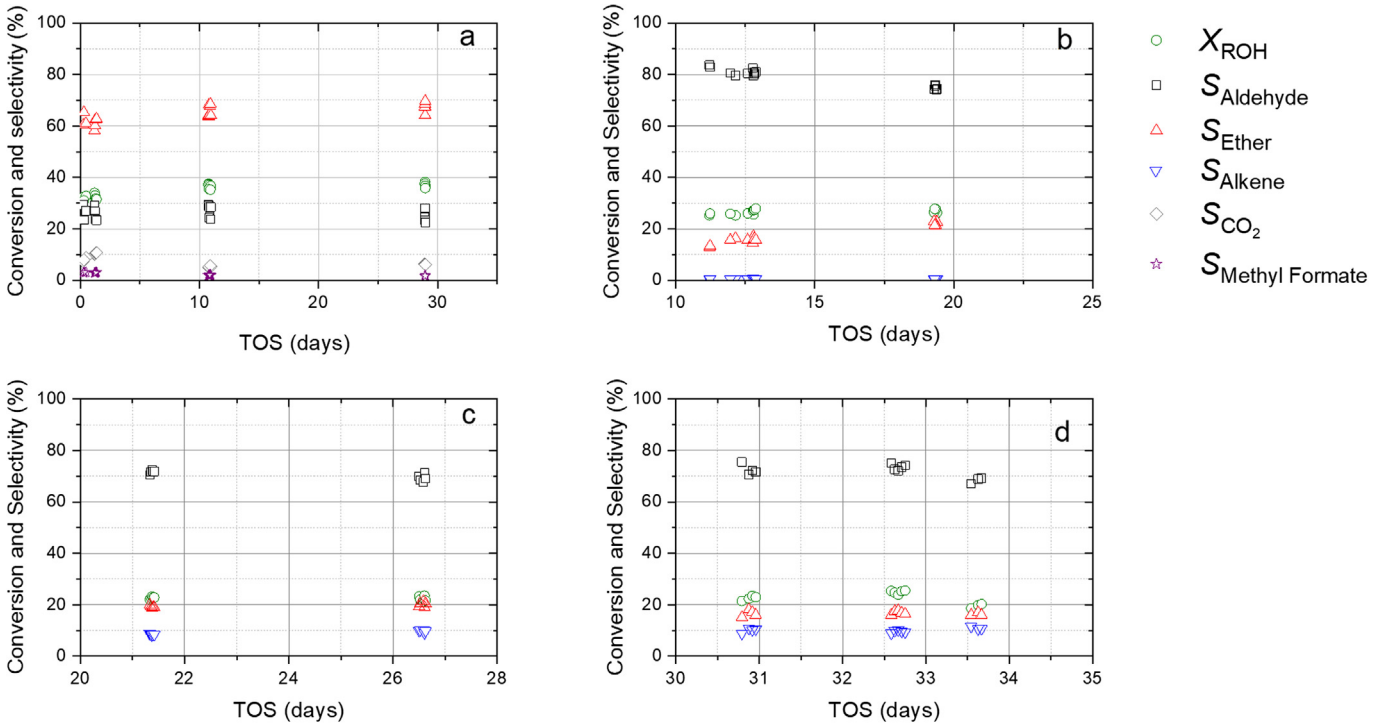

Fig. 6. Results of the stability tests over coating 1 in (a) methanol (b) ethanol (c) propanol and (d) butanol oxidation.

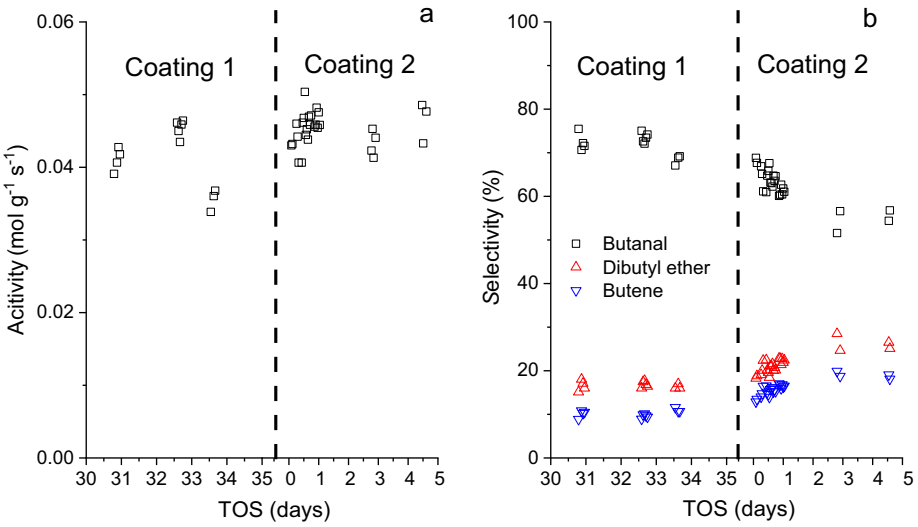

Fig. 7. Repeatability tests in butanol oxidation. (a) Turnover frequency vs TOS (b) product distribution vs TOS.

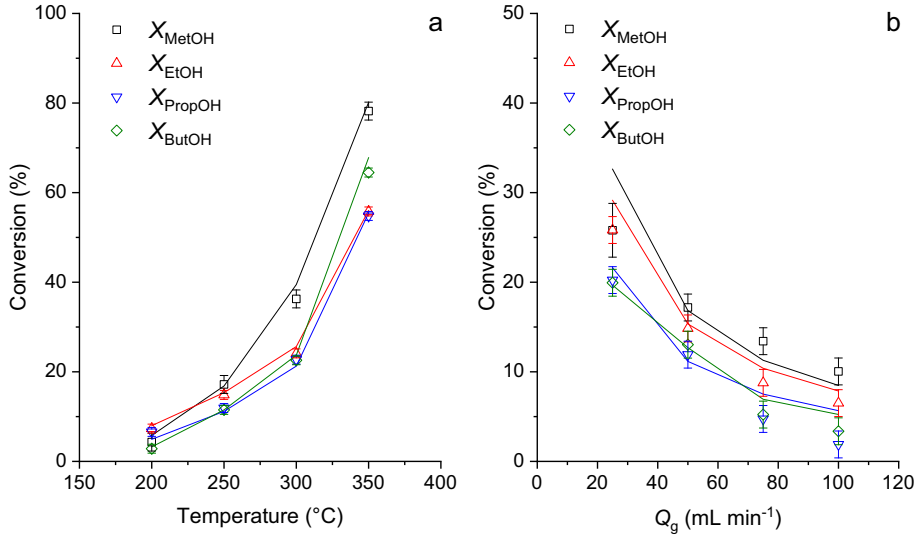

Fig. 8. Alcohol conversion a function of (a) temperature (b) total volumetric flow rate. Symbols represent the experimental data while solid lines reflect the simulated values.

gold with the chain length (Table 4). Here, it was found that the effect of the alcohol chain length increase is not significant after propanol.

A high reactivity of formaldehyde in the subsequent transformations led to a more rapid decreasing profile of its selectivity (Fig. 9a). On the contrary, acetaldehyde displayed a high selectivity at all temperatures investigated. Alcohol dehydration is more sensitive to temperature rise than etherification as the activation energy of the latter is lower (Phung et al.,2014, Clayborne et al., 2004). As a result, selectivity to propene and butene is 40 % at 350 °C.

Methanol conversion is enhanced in diluted systems (Fig. 10a), which reflects strong adsorption of the alcohol on the catalyst surface. The conversion was experimentally observed to be independent of the oxygen-to-methanol ratio (Fig. 10a). Since methyl formate and CO_2 formation is negligible at 250 °C, it was revealed that the reaction order of oxygen in formaldehyde formation is zero. This finding is in agreement with the work of Pestryakov et al., 2013, who ascribed the zero-order kinetics with respect to oxygen at the kinetic control of methanol oxidation on gold nanoparticles.

On the contrary, ethanol, propanol and butanol conversion was improved by the oxygen concentration in the feed. Lateral interactions between the adsorbed oxygen and alcohol on the catalytic surface might lead to different adsorption strength of the oxygen on gold, changing the influence of the oxygen concentration on the alcohol conversion. Mathematical modelling confirmed that the adsorption constant of oxygen on gold surface decreases as the chain length increase (Table 4). Alcohol concentration in the feed did not improve conversion significantly for oxidation of ethanol, propanol and butanol (Fig. 10b-10d).

Since the reaction order in oxygen is zero with respect to selective oxidation, the formaldehyde selectivity did not show any trend with the oxygen-to-alcohol molar ratio (Fig. 11a). As oxygen does not take part in dehydration reactions and total oxidation was not observed, oxygen concentration improved selectivity to aldehyde in ethanol, propanol and butanol oxidation (Fig. 11b-11d).

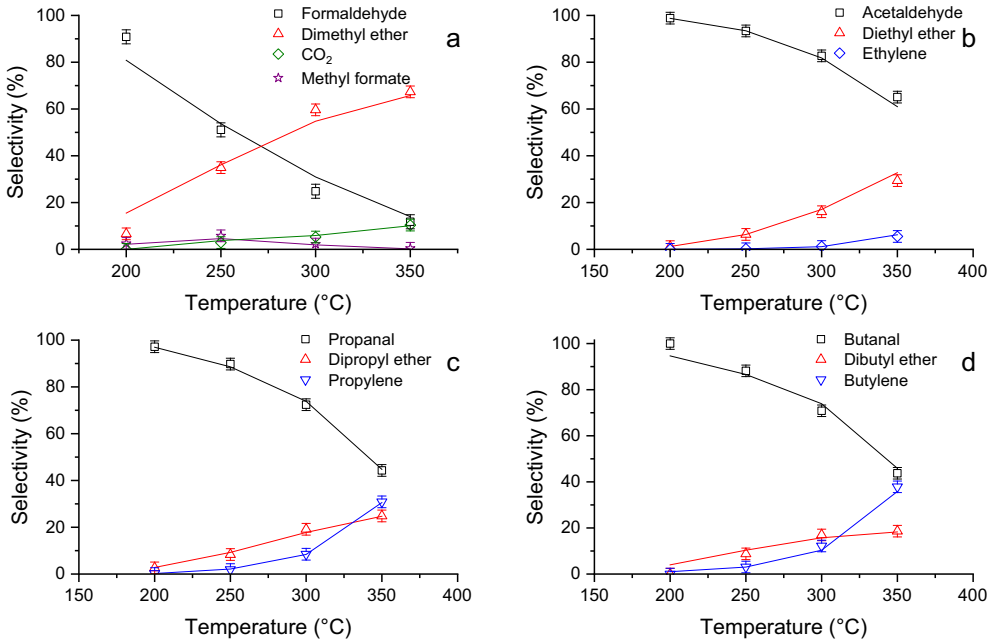

Fig. 9. Product distribution in (a) methanol (b) ethanol (c) propanol and (d) butanol oxidation as a function of temperature. Symbols represent the experimental data while solid lines reflect the simulated values.

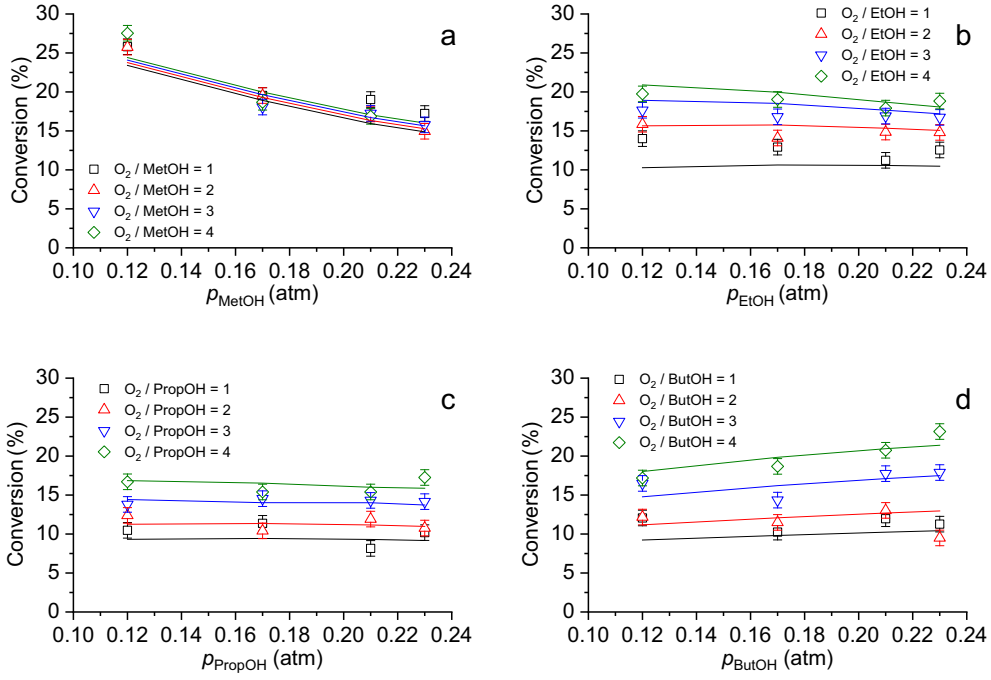

Fig. 10. Effect of alcohol concentration and oxygen-to-alcohol molar ratio on conversion in oxidation of (a) methanol (b) ethanol (c) propanol and (d) butanol. Symbols represent the experimental data while solid lines reflect the simulated values.

4. Kinetic modelling principles and results

4.1. Modelling principles

The modelling principles are based on the consideration of the reactor flow pattern, mass transfer effects in the catalyst layer, as well as thermodynamic and kinetic considerations. The ultimate goal is to determine meaningful numerical values for the rate and adsorption parameters included in the kinetic model.

4.1.1. Pseudo-homogeneous plug-flow model

The Reynolds number (*Re*) is typically very low in microreactors, giving a clear indication of a laminar flow inside the microchannels. However, the spreading effect of a laminar velocity profile is counterbalanced by the extremely rapid molecular diffusion because of the micrometre dimension of the microchannels. Indeed, the Pèclet number is very high (>100), making the plug flow assumption very solid for the flow pattern even if the mixing relies on diffusion only (Jess and Wasserscheid, 2013).

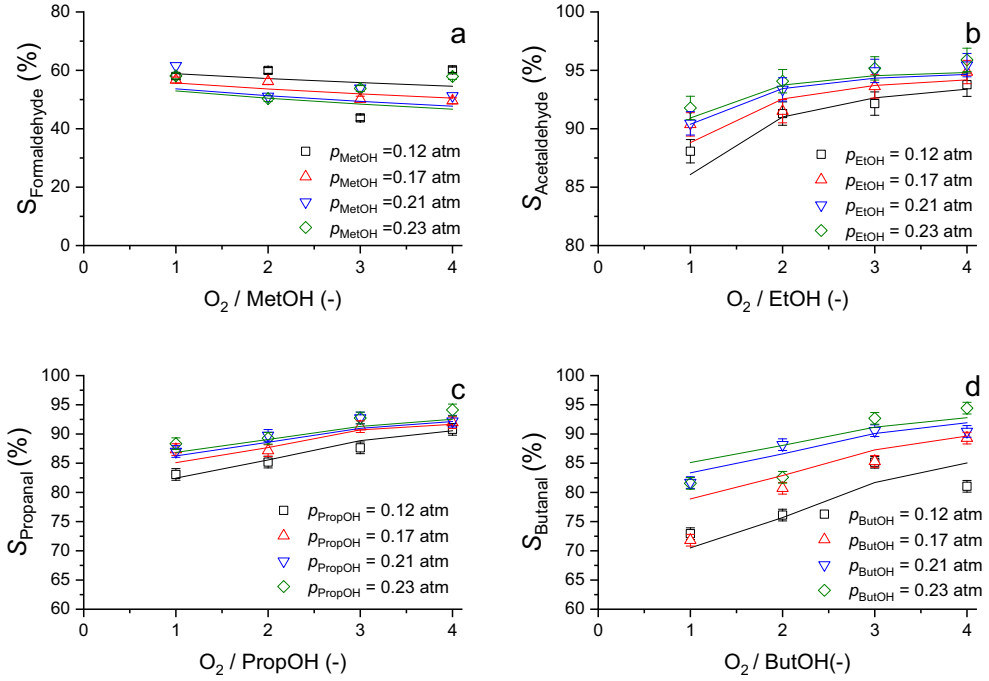

Fig. 11. Effect of alcohol concentration and oxygen-to-alcohol molar ratio on selectivity to aldehyde in oxidation of (a) methanol (b) ethanol (c) propanol and (d) butanol. Symbols represent the experimental data while solid lines reflect the simulated values.

Assuming constant volumetric flow rate within the microchannels, the mass balance under steady-state conditions is written as displayed below.

$$\frac{u_g}{L_r}\frac{dC_i}{dx} = \rho_b \sum_{j=1}^{N_R} v_{ij} r_j \tag{1}$$

where u_g is the gas velocity, v_{ij} is element of the stoichiometric matrix, L_r is the length of the microreactor channel and ρ_b is the bulk density, i.e. the mass of catalyst (w_{cat})-to-reactor volume ratio. At $\times$ = 0, the concentration of the component i is equal to the inlet concentration. Therefore, the inlet condition is.

$$C_i|_{x=0} = C_{0,i} \tag{2}$$

4.1.2. Intrawashcoat diffusion model

For extremely rapid reactions, diffusion inside the coating layer might have a retarding effect and intrawashcoat concentration profiles might arise. Therefore, the concentration profiles inside the catalytic washcoat layer were monitored with the aid of a combined kinetic and mass transport model. The steady state mass balance equations for the fluid and the solid phase are written as Eqs. (3) and (4), respectively.

$$\frac{u_g}{L_r}\frac{dC_i(x)}{dx} = \frac{D_{eff,i}}{R_w^2}\frac{\partial C_{s,i}(x,\chi)}{\partial \chi}\bigg|_{\chi=0} \tag{3}$$

$$\frac{D_{eff,i}}{R_w^2}\left(\frac{\partial^2 C_{s,i}(x,\chi)}{\partial \chi^2} + \frac{s}{\chi}\frac{\partial C_{s,i}(x,\chi)}{\partial \chi}\right) + \sum_{j=1}^{N_R} v_{ij} r_j = 0 \tag{4}$$

The radial concentration profiles in the gas bulk phase were considered to be negligible. However, concentration gradients inside the coating layer might arise because of the diffusion resistance inside the catalyst layer. Under steady state conditions, the convective flux in the bulk is equal to the molecular flux at the washcoat inlet (χ = 0).

In the catalytic layer, the mass transport relies on the diffusion only, but chemical reactions proceed simultaneously there. The boundary conditions of the coupled system of partial and ordinary differential equations are listed in Eqs. (5),

$$C_i(x)|_{x=0} = C_{i,0} \tag{5a}$$

$$C_i(x) = C_{s,i}(x,\chi)\big|_{\chi=0} \tag{5b}$$

$$\frac{\partial C_{s,i}(x,\chi)}{\partial \chi}\bigg|_{\chi=1} = 0 \tag{5c}$$

At the microreactor inlet (x = 0), the boundary condition is the same as in the plug flow model (Eq. (2)). As the impact of the film resistance to the mass transfer can be neglected in gas-phase systems, the concentration in the solid phase at χ = 0 is equal to the bulk concentration. Because the gas cannot diffuse through the reactor wall, the first derivative of the concentration in the solid is 0 at χ = 1.

4.1.3. Thermodynamic calculations

The Gibbs energy and enthalpy of formation at standard conditions were employed to estimate standard enthalpy and Gibbs energy of the reactions, according to Eqs. 6–7.

$$\Delta_r H_j^0 = \sum_j v_{ij} \cdot \Delta_f H_i^0 \tag{6}$$

$$\Delta_r G_j^0 = \sum_j v_{ij} \cdot \Delta_f G_i^0 \tag{7}$$

The temperature dependence of the Gibbs energy was evaluated according to the Gibbs-Helmholtz equation.

$$\frac{\Delta_r G_j(T)}{T} = \frac{\Delta_r G_j^0}{T^0} + \Delta_r H_j^0\left(\frac{1}{T} - \frac{1}{T^0}\right) \tag{8}$$

Finally, the equilibrium constant was calculated applying the van't Hoff equation.

$$K_{eq,j}(T) = \exp\left[-\frac{\Delta_r G_j(T)}{RT}\right] \quad (9)$$

The results of the thermodynamic calculations for each substrate are reported in the Supplementary material (Tables S2-S9).

4.1.4. Numerical strategies

A coupled system of partial and differential equations (PDEs) appeared in the development of the intrawashcoat diffusion model (Eqs. 3–4), which was numerically solved by the method of lines (MOL) algorithm included in gPROMS ModelBuilder v.4.0.0 software. The MOL discretizes the spatial domains while the time variable is left continuous, converting the PDEs in a large set of ODEs. The backward finite difference formulae and the central difference formulae were applied as the methods of discretization for the first and second derivatives, respectively.

To perform the parameter estimation the solver MAXLKHD, included in the gPROMS software, was employed. It is based on a maximum likelihood approach, implying that the values of the unknown parameter are determined to maximize the probability that the model will describe the experimental values given as an input to the system.

4.2. Rate equations

The reaction rate equations were developed based on the experimental findings. The mathematical formulation of them is summarized in Table 3. The kinetic expression of alcohol selective oxidation is in line with the mechanism proposed based on DFT calculations for ethanol oxidative dehydrogenation on gold (Behravesh et al., 2021), where K^G_{ROH} and $K^G_{O_2}$ are the adsorption constants of alcohol and oxygen on the gold surface, respectively.

Table 3
Kinetic equations.

Methanol	Ethanol, propanol and butanol
$r_{ALDE}=\frac{k'_{ALDE}C_{MetOH}}{1+K^G_{MetOH}C_{MetOH}}$	$r_{ALDE}=\frac{k'_{ALDE}C_{ROH}C_{O_2}}{(1+K^G_{ROH}C_{ROH}+K^G_{O_2}C_{O_2})^2}$
$r_{ET}=\frac{k'_{ET}\left(C^2_{MetOH}-C_{DME}C_W/K_{eq,DME}\right)}{(1+K^L_{MetOH}C_{MetOH})^2}$	$r_{ET}=\frac{k'_{ET}\left(C^2_{ROH}-C_{ET}C_W/K_{eq,ET}\right)}{(1+K^L_{ROH}C_{ROH})^2}$
$r_{CO_2}=\frac{k'_{CO_2}C_{ROH}C_{O_2}}{1+K^G_{MetOH}C_{MetOH}}$	$r_{ALK}=\frac{k'_{ALK}C_{ROH}}{1+K^L_{ROH}C_{ROH}}$
$r_{MF}=\frac{k'_{MF}C_{ROH}C_{O_2}C_{FA}}{1+K^G_{MetOH}C_{MetOH}}$	
$r_{DEC}=k_{DEC}C_{MF}$	

Since a zero-order kinetics was observed in formaldehyde formation, the oxygen dependence in formaldehyde formation was discarded. The adsorption constant K^L_{ROH} is referred to the adsorption of the alcohol on Lewis acid sites, which are active in etherification. The active sites catalyzing alkene formation are still debated: some authors reported that Lewis sites are involved in the alkene formation (Phung et al., 2014), others that it takes place mainly on Brønsted sites (Suerz et al., 2021). As alkene selectivity is low in most of the experiments, it is not possible to discriminate between these two assumptions. To minimize the number of parameters in the kinetic modelling, alkene formation was supposed to occur on Lewis acid sites. Moreover, the desorption of the reaction products was discarded. First-order kinetics was assumed for the thermal decomposition of methyl formate (Francisco, 2003). Etherification equilibrium constants were calculated based on the thermodynamic approach reported in the supplementary material. The values are listed in Tables S8-S9.

The dependence of the kinetic constants on the reaction temperature was taken into account implementing the modified Arrhenius law (Murzin and Salmi, 2016).

$$k_j = k_{ref,j}e^{-\frac{E_{a,j}}{R}\left(\frac{1}{T}-\frac{1}{T_{ref}}\right)} \quad (11)$$

where $k_{ref,j}$ is the value of the kinetic constant at the reference temperature T_{ref} = 250 °C. The modification of the Arrhenius law was used to suppress the correlation between the activation energy and the pre-exponential factor.

4.3. Parameter estimation results

The rate expressions listed in Table 4 were implemented in the pseudo-homogeneous plug flow model (Eq. (1)) to estimate the kinetic parameters.

In general, the experimental trends were successfully predicted (Figs. 8-11), with a coefficient of determination $R^2 > 0.985$ for each substrate. The normal distributions of the residuals were revealed from the parity plots displayed in Fig. 12, where the kinetic model predicted the experimental values within a confidence interval of 20 %.

Fig. 11d indicates that the experimental values at oxygen-to-butanol ratio equal to 1 differ from the predicted values. This was ascribed to the small catalyst deactivation in butanol oxidation (Fig. 7b). Indeed, the experiments with stoichiometric amounts of oxygen were conducted at the end of the experimental campaign, hence the selectivity values were slightly overestimated

Table 4
Estimated kinetic parameters.

Parameter	Unit	Value ± 95 % CI			
		Methanol	Ethanol	Propanol	Butanol
$E_{a,Alde}$	kJ mol^{-1}	23 ± 3	25 ± 2	29 ± 2	44 ± 2
$E_{a,Et}$	kJ mol^{-1}	76 ± 4	93 ± 2	81 ± 2	76 ± 1
$E_{a,Alk}$	kJ mol^{-1}	/	129 ± 2	123 ± 4	124 ± 2
$E_{a,CO2}$	kJ mol^{-1}	81 ± 2	/	/	/
$E_{a,MF}$	kJ mol^{-1}	74 ± 5	/	/	/
$E_{a,Dec}$	kJ mol^{-1}	103 ± 16	/	/	/
$k_{ref,Alde}$	m^6/(kg mol s)	0.11 ± 0.03*	$2{\cdot}10^{-2} \pm 4{\cdot}10^{-3}$	$1{\cdot}10^{-2} \pm 3{\cdot}10^{-3}$	$5{\cdot}10^{-3} \pm 8{\cdot}10^{-4}$
$k_{ref,Et}$	m^6/(kg mol s)	0.08 ± 0.08	$4{\cdot}10^{-3} \pm 2{\cdot}10^{-3}$	$2{\cdot}10^{-3} \pm 1{\cdot}10^{-3}$	$3{\cdot}10^{-2} \pm 2{\cdot}10^{-2}$
$k_{ref,Alk}$	m^3/(kg s)	/	$4{\cdot}10^{-4} \pm 1{\cdot}10^{-4}$	$2{\cdot}10^{-2} \pm 1{\cdot}10^{-3}$	$1{\cdot}10^{-2} \pm 5{\cdot}10^{-3}$
$k_{ref,CO2}$	m^6/(kg mol s)	$8{\cdot}10^{-4} \pm 2{\cdot}10^{-4}$	/	/	/
$k_{ref,MF}$	m^9/(kg mol^2 s)	$2{\cdot}10^{-3} \pm 6{\cdot}10^{-4}$	/	/	/
$k_{ref,dec}$	m^3/(kg s)	0.46 ± 0.05	/	/	/
$K^G_{O_2}$	m^3/mol	/	0.07 ± 0.01	0.04 ± 0.01	$9{\cdot}10^{-3} \pm 5{\cdot}10^{-3}$
K^G_{ROH}	m^3/mol	0.5 ± 0.2	0.08 ± 0.01	0.1 ± 0.03	0.04 ± 0.02
K^L_{ROH}	m^3/mol	1 ± 0.6	0.6 ± 0.2	0.4 ± 0.1	1.7 ± 1

* in methanol oxidation, the unit of $k_{ref,Alde}$ is m^3/(kg s).

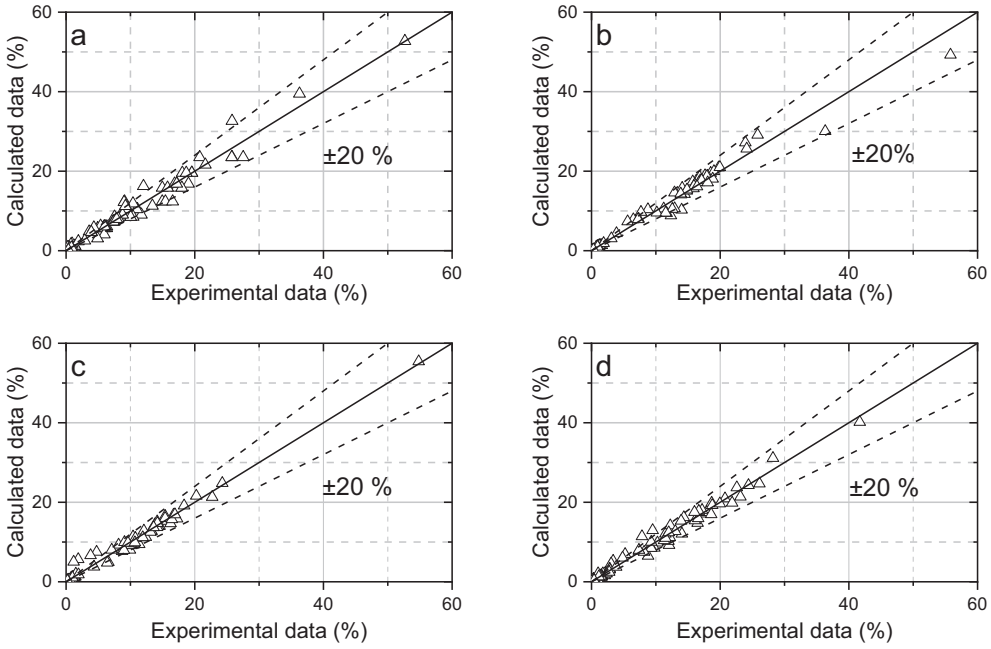

Fig. 12. Parity plots for (a) methanol (b) ethanol (c) propanol (d) butanol oxidation. The data are expressed as percentage yield and conversion.

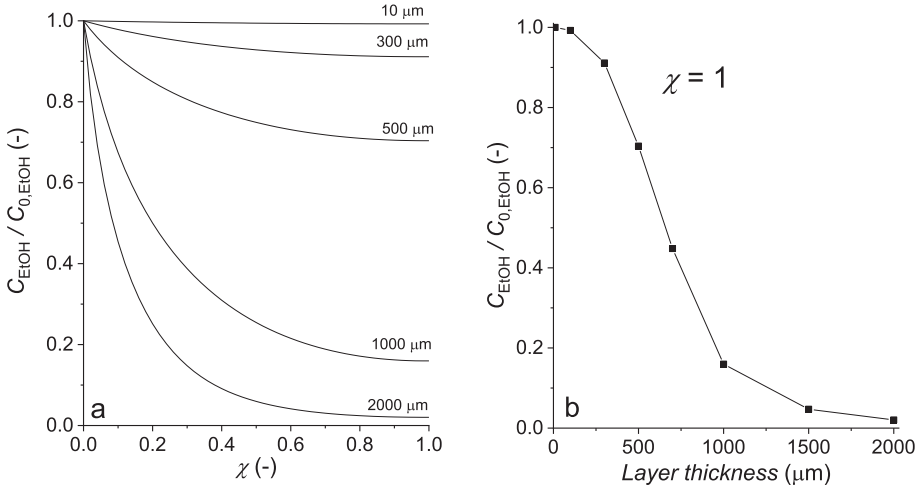

Fig. 13. Intrawashcoat concentration profile of ethanol at different catalytic layer thicknesses (b) dimensionless concentration vs layer thickness at χ = 1.

from the kinetic model. The model fit for the oxygen-rich systems is considered to be acceptable.

The activation energy of the selective oxidation of alcohol increases as the alcohol chain length increases (Table 4). Furthermore, it shows values below 30 kJ mol^{-1} except from butanal formation, probably because of the activation energy dependence on nanocluster size for structure-sensitive catalysts (Murzin, 2019). Alcohol dehydration and etherification revealed estimated activation energies consistent with previous findings on pure alumina (Roy et al., 2012, Kostestkyy et al., 2014, Swecker and Datye, 1990). The kinetic modelling confirmed that the alcohol adsorption coefficient on both gold and Lewis sites decreases with the chain length.

4.4. Concentration profiles inside the washcoat layer

Ethanol oxidation was chosen as the reference reaction to implement the intrawashcoat diffusion model. The temperature was set at 350 °C to simulate conditions in which is more likely that a concentration gradient in the washcoat layer is established.

The binary molecular diffusivities were calculated with the Fuller-Schettler-Giddings equation (Schettler and Giddings, 1966).

$$D_{A,B}\left[\frac{cm^2}{mol}\right] = \frac{10^{-3}T^{1.75}\left(\frac{1}{M_A}+\frac{1}{M_B}\right)^{\frac{1}{2}}}{p\left[\left(\sum v_A\right)^{1/3}+\left(\sum v_B\right)^{1/3}\right]^2} \quad (12)$$

where $\Sigma\ v_i$ is the sum of the atomic diffusion volume increments of the component *i*. To have a reasonable order of magnitude, the effective diffusion coefficient was estimated as one-tenth of the molecular one.

The ethanol concentration profiles inside the washcoat at different thicknesses of the coating layer are displayed in Fig. 13.

The simulation confirmed that no concentration gradients arise in catalytic layers below 10 μm but the diffusion limitations are severe for layers thicker than 300 μm. As it was mentioned above,

the thickness of the catalyst layer in the current work was 8 ± 1 μm. Typically, the catalyst layer in a microreactor does not exceed 30 μm: thus, in this case it is possible to consider flat concentrations inside the catalytic washcoat when using microreactors. Nevertheless, diffusion inside the coating layer might become a limiting factor in milli-structured devices. To sum up, the intrawashcoat diffusion model have been a useful tool to strengthen the assumption of plug flow in the microreactor.

5. Conclusions

Selective oxidation of methanol, ethanol, propanol and butanol was performed successfully in a microreactor. Gold nanoparticles, dispersed on γ-alumina, were used as the catalyst coated in the microreactor channels.

The slurry-based method was successfully employed to coat the microreactor channels. Nanoparticle distribution size, acidity, specific surface area and the average pore size of the catalyst were evaluated as well as the uniformity and thickness of the washcoat layer.

The effect of temperature, residence time and the reactant concentrations on both the alcohol conversion and product distribution were investigated in depth. The experiments revealed a decline of catalytic activity with the alcohol chain length ranging from one to three carbon atoms. Propanol and butanol showed similar catalytic activities.

The collected experimental data were used in the modelling of the microreactor. Mechanistically sound rate expressions were implemented in a pseudo-homogeneous plug flow model to estimate the kinetic parameters. The importance of the molecular diffusion inside the catalytic layer was investigated with an advanced reaction–diffusion model, confirming the excellent properties of microreactors in suppressing the internal transport limitations in catalyst layers.

CRediT authorship contribution statement

Luca Mastroianni: Data curation, Investigation, Methodology, Visualization, Software, Writing – original draft. **Zuzana Vajglová:** Methodology, Investigation, Visualization. **Kari Eränen:** Project administration, Resources, Software, Supervision. **Markus Peurla:** Investigation, Validation, Visualization. **Martino Di Serio:** Conceptualization, Supervision, Validation. **Dmitry Yu. Murzin:** Conceptualization, Supervision, Writing – review & editing. **Vincenzo Russo:** Conceptualization, Supervision, Software, Writing – review & editing. **Tapio Salmi:** Conceptualization, Methodology, Project administration, Resources, Software, Supervision, Writing – review & editing.

Data availability

Data will be made available on request.

Declaration of Competing Interest

The authors declare that they have no known competing financial interests or personal relationships that could have appeared to influence the work reported in this paper.

Acknowledgements

This research effort is a part of the activities financed by Academy of Finland, the Academy Professor grants 319002, 320115, 345053 (Tapio Salmi and Luca Mastroianni). We are grateful to the Electron Microscopy Laboratory, Institute of Biomedicine, University of Turku, and Biocenter Finland for the TEM investigations.

Appendix A. Supplementary material

Supplementary data to this article can be found online at https://doi.org/10.1016/j.ces.2022.117920.

References

Abad, A., Corma, A., García, H., 2008. Catalyst Parameters Determining Activity and Selectivity of Supported Gold Nanoparticles for the Aerobic Oxidation of Alcohols: The Molecular Reaction Mechanism. Chem. Eur. J. 14 (1), 212–222.
Behravesh, E., Kumar, N., Balme, Q., Roine, J., Salonen, J., Schukarev, A., Mikkola, J.-P., Peurla, M., Aho, A., Eränen, K., Murzin, D.Y., Salmi, T., 2017. Synthesis and characterization of Au nano particles supported catalysts for partial oxidation of ethanol: influence of solution pH, Au nanoparticle size, support structure and acidity. J. Catal. 353, 223–238.
Behravesh, E., Kilpiö, T., Russo, V., Eränen, K., Salmi, T., 2018. Experimental and modelling study of partial oxidation of ethanol in a micro-reactor using gold nanoparticles as the catalyst. Chem. Eng. Sci. 176, 421–428.
Behravesh, E., Eränen, K., Kumar, N., Peltonen, J., Peurla, M., Nurmi, M., Toivakka, M., Murzin, D.Y., Salmi, T., 2019. Microreactor coating with Au/Al_2O_3 catalyst for gas phase partial oxidation of ethanol: physico-chemical evaluation and evaluation of catalytic properties. Chem. Eng. J. 378, 122179.
Behravesh, E., Melander, M.M., Wärnå, J., Salmi, T., Honkala, K., Murzin, D.Y., 2021. Oxidative dehydrogenation of ethanol on gold: Combination of kinetic experiments and computation approach to unravel the reaction mechanism. J. Catal. 394, 193–205.
Boronat, M., Corma, A., Illas, F., Radilla, J., Ródenas, T., Sabater, M.J., 2011. Mechanism of selective alcohol oxidation to aldehydes over gold catalysts: Influence of surface roughness on reactivity. J. Catal. 278, 50–58.
Clayborne, P.A., Nelson, T.C., DeVore, T.C., 2004. Temperature programmed desorption-FTIR investigation of C_1–C_5 primary alcohols adsorbed on γ-alumina. App. Catal. A: Gen. 257, 225–233.
Corma, A., Garcia, H., 2008. Supported gold nanoparticles as catalysts for organic reactions. Chem. Soc. Rev. 37 (9), 2096. https://doi.org/10.1039/b707314n.
Dong, Z., Wen, Z., Zhao, F., Kuhn, S., Noël, T., 2021. Scale-up of micro- and milli-reactors: An overview of strategies, design principles and applications. Chem. Eng. Sci. 10, 100097. https://doi.org/10.1016/j.cesx.2021.100097.
Emeis, C.A., 1993. Determination of integrated molar extinction coefficients for infrared absorption bands of pyridine adsorbed on solid acid catalysts. J. Catal. 141 (2), 347–354.
Fokin, S.J., 1913. Catalytic oxidation reaction at high temperatures. J. Russ. Phys. Chem. Soc. 45, 286–288.
Francisco, J.S., 2003. Mechanicistic Study of the Gas-Phase Decomposition of Methyl Formate. J. Am. Chem. Soc. 125, 10475–10480.
Gong, H., Chuan, Z., Yan, C., Sheng, D., Xiuge, Z., Ruihan, L., Pengfei, A., Huan, L., Haifeng, W., Zhenshan, H., 2020. Direct transforamation of glycerol to propanal using zirconium phosphate-supported bimetallic catalysts. ChemSusChem 13, 4954–4966.
Jess, A., Wasserscheid, P., 2013. Chemical Technology: An Integrated Textbook. Wiley-VCH, Weinheim.
Kostestkyy, P., Yu, J., Gorte, R.J., Mpourmpakis, G., 2014. Structure-activity relationships on metal oxides: alcohol dehydration. Catal. Sci. Technol. 4 (11), 3861–3869.
Mascal, M., 2012. Chemicals from biobutanol: technologies and markets. Biofuels, Bioprod. Bioref. 6 (4), 483–493.
Murzin, D.Y., 2019. On Apparent activation energy of structure sensitive heterogeneous catalytic Reactions. Catal. Lett. 149 (6), 1455–1463.
Murzin, D.Y., Salmi, T., 2016. Catalytic Kinetics: Chemistry and Engineering. Elsevier Science, Amsterdam.
Pestryakov, A.N., Lunin, V.V., Bogdanchikova, N., Temkin, O.N., Smolentseva, E., 2013. Active states of gold in small and big metal particles in CO and methanol selective oxidation. Fuel 110, 48–53.
Phung, T.K., Lagazzo, A., Rivero Crespo, M.Á., Sánchez Escribano, V., Busca, G., 2014. A study of commercial transition aluminas and of their catalytic activity in the dehydration of ethanol. J. Catal. 311, 102–113.
Roy, S., Mpourmpakis, G., Hong, D., Dionisios, G.V., Bhan, A., Gorte, R.J., 2012. Mechanicistic Study of Alcohol Dehydration on γ-Al_2O_3. ACS Catal. 2, 1846–1853.
Salmi, T., Mikkola, J.P., Wärnå, J., 2019. Chemical Reaction Engineering and Reactor Technology. Taylor&Francis Group CRC Press, Boca Raton Florida.
Salthammer, T., Mentese, S., Marutzky, R., 2010. Formaldehyde for indoor environment. Chem. Rev. 110, 2536–2572.
Schettler, P.D., Giddings, J.C., 1966. New method for prediction of binary gas-phase diffusion coefficients. Ind. Eng. Chem. Res. 58 (5), 18–27.
Schmidt, S.A., Kumar, N., Zhang, B., Eränen, K., Murzin, D.Y., Salmi, T., 2012. Preparation and Characterization of Alumina-Based Microreactors for Application in Methyl Chloride Synthesis. Ind. Eng. Chem. Res 51 (12), 4545–4555.

Schmidt, S.A., Kumar, N., Reinsdorf, A., Eränen, K., Wärnå, J., Murzin, D.Y., Salmi, T., 2013. Methyl chloride synthesis over Al_2O_3 catalyst coated microstructured reactor-Thermodynamics, kinetics and mass transfer. Chem. Eng. Sci. 95, 232–245.

Sharma, A.S., Kaur, H., Shah, D., 2016. Selective oxidation of alcohols by supported gold nanoparticles: recent advances. RSC Adv. 6 (34), 28688–28727.

Sheldon, R.A., Arends, I.W.C.E., ten Brink, G.-J., Dijksman, A., 2002. Green, Catalytic Oxidations of Alcohols. Acc. Chem. Res. 35 (9), 774–781.

Simakova, O.A., Kusema, B.T., Campo, B.C., Leino, A., Kordás, K., Pitchon, V., Mäki-Arvela, P., Murzin, D., 2011. Structure Sensitivity in L-Arabinose Oxidation over Au/Al_2O_3 Catalysts. J. Phys. Chem. 115, 1036–1043.

Suerz, R., Eränen, K., Kumar, N., Wärnå, J., Russo, V., Peurla, M., Aho, A., Murzin, D. Yu., Salmi, T., 2021. Application of microreactor technology to dehydration of bio-ethanol. Chem. Eng. Sci. 229, 116030. https://doi.org/10.1016/j.ces.2020.116030.

Swecker, J.L., Datye, A.K., 1990. Alcohol Dehydration over Model Nonporous Alumina Powder. J. Catal. 121, 196–201.

Tabakova, T., 2019. Recent advances in design of gold-based catalysts for H_2 clean-up reactions. Front. Chem. 7, 1–24.

Vajglová, Z., Kumar, N., Eränen, K., Peurla, M., Murzin, D.Y., Salmi, T., 2018. Ethene oxychlorination over $CuCl_2/\gamma$-Al_2O_3 catalyst in micro- and millistructured reactors. J. Catal. 364, 334–344.

Wang, F., Ueda, W., 2008. Aerobic oxidation of alcohols over novel crystalline Mo-V-O oxide. Appl. Cat. A: Gen. 346 (1-2), 155–163.

Xu, J., Xu, X.-C., Yang, X.-J., Han, Y.-F., 2016. Silver/hydroxyapatite foam as a highly selective catalyst for acetaldehyde production via ethanol oxidation. Catal. Today 276, 19–27.